

Defect of Mitotic Vimentin Phosphorylation Causes Microphthalmia and Cataract via Aneuploidy and Senescence in Lens Epithelial Cells*[♦]

Received for publication, August 29, 2013, and in revised form, October 11, 2013. Published, JBC Papers in Press, October 18, 2013, DOI 10.1074/jbc.M113.514737

Makoto Matsuyama^{‡1}, Hiroki Tanaka^{‡1}, Akihito Inoko^{‡1}, Hidemasa Goto^{‡§}, Shigenobu Yonemura[¶], Kyoko Kobori[‡], Yuko Hayashi[‡], Eisaku Kondo^{||**}, Shigeyoshi Itoharu^{‡‡}, Ichiro Izawa[‡], and Masaki Inagaki^{‡§2}

From the Divisions of [‡]Biochemistry and ^{||}Oncological Pathology, Aichi Cancer Center Research Institute, Nagoya, Aichi 464-8681, the Departments of [§]Cellular Oncology and ^{**}Epidemiology, Nagoya University Graduate School of Medicine, Nagoya, Aichi 466-8550, the [¶]Electron Microscope Laboratory, RIKEN Center for Developmental Biology, Kobe, Hyogo 650-0047, and the ^{‡‡}Laboratory for Behavioral Genetics, RIKEN Brain Science Institute, 2-1 Hirosawa, Wako 351-0198, Japan

Background: Vimentin, an intermediate filament (IF) protein, is phosphorylated in mitosis.

Results: Disruption of vimentin phosphorylation during cell division leads to chromosomal instability (CIN) and premature aging in mouse lens tissue.

Conclusion: Our data document the first physiological importance of vimentin phosphorylation during mitosis for organogenesis and tissue homeostasis.

Significance: Our data suggest a possible causal relationship between CIN and premature aging.

Vimentin, a type III intermediate filament (IF) protein, is phosphorylated predominantly in mitosis. The expression of a phosphorylation-compromised vimentin mutant in T24 cultured cells leads to cytokinetic failure, resulting in binucleation (multinucleation). The physiological significance of intermediate filament phosphorylation during mitosis for organogenesis and tissue homeostasis was uncertain. Here, we generated knock-in mice expressing vimentin that have had the serine sites phosphorylated during mitosis substituted by alanine residues. Homozygotic mice ($VIM^{SA/SA}$) presented with microphthalmia and cataracts in the lens, whereas heterozygotic mice ($VIM^{WT/SA}$) were indistinguishable from WT ($VIM^{WT/WT}$) mice. In $VIM^{SA/SA}$ mice, lens epithelial cell number was not only reduced but the cells also exhibited chromosomal instability, including binucleation and aneuploidy. Electron microscopy revealed fiber membranes that were disorganized in the lenses of $VIM^{SA/SA}$, reminiscent of similar characteristic changes seen in age-related cataracts. Because the mRNA level of the senescence (aging)-related gene was significantly elevated in samples from $VIM^{SA/SA}$, the lens phenotype suggests a possible causal relationship between chromosomal instability and premature aging.

Intermediate filaments (IFs),³ together with microtubules and actin filaments, form the cytoskeletal framework in the cytoplasm of various eukaryotic cells. IF proteins are divided into six groups related to their primary sequence characteristics, their tissue-specific expression profiles, and differentiation status (1–3). For example, GFAP and desmin are type III IF proteins that are expressed specifically in astroglial and muscular cells, respectively (4–6). However, vimentin, another type III IF protein, is expressed in all mesenchymal cells with the eye lens being the tissue with by far the highest levels (7, 8).

There is increasing evidence that IF disassembly is regulated by phosphorylation of Ser/Thr residues in the amino-terminal head domain on IF proteins (9, 10). The first direct evidence was obtained by an *in vitro* study that treated polymerized vimentin filaments with a purified protein kinase to cause their disassembly (11). Site- and phosphorylation state-specific antibodies that can recognize a phosphorylated residue and its flanking sequence (12, 13) are powerful tools able to resolve the spatial and temporal details of IF phosphorylation in cells (14, 15). Using antibodies raised against four distinct phosphorylation sites in GFAP, we showed that mitotic IF phosphorylation is regulated by different protein kinases in a spatiotemporal manner (13, 16). Further detailed studies revealed that several mitotic kinases, such as Aurora-B (17, 18), Cdk1 (19, 20), Plk1 (21), and Rho kinase (22–24), participate in the phosphorylation of type III IF proteins during cell division. By transient expression of type III IF proteins mutated at these mitotic phosphorylation sites to Ala, we found that preventing the phosphorylation of IFs during cell division inhibited cytokinesis by the retention of an IF bridge that connected the two daughter cells

* This work was supported in part by grants-in-aid for scientific research from the Japan Society for the Promotion of Science and from the Ministry of Education, Science, Technology, Sports and Culture of Japan, a grant-in-aid for the Third Term Comprehensive 10-Year Strategy for Cancer Control from the Ministry of Health and Welfare, Japan, the Uehara Memorial Foundation, the Naito Foundation, a research grant from the Princess Takamatsu Cancer Research Fund, and the Takeda Science Foundation.

✂ Author's Choice—Final version full access.

♦ This article was selected as a Paper of the Week.

¹ These authors contributed equally to this work.

² To whom correspondence should be addressed: Division of Biochemistry, Aichi Cancer Center Research Institute, 1-1 Kanokoden, Chikusa-ku, Nagoya, Aichi 464-8681, Japan. Tel.: 81-52-762-6111 (Ext. 7020); Fax: 81-52-763-5233; E-mail: minagaki@aichi-cc.jp.

³ The abbreviations used are: IF, intermediate filament; AQP0, aquaporin 0; CIN, chromosomal instability; GFAP, glial fibrillary acidic protein; MIP, membrane intrinsic protein; Ndr2, N-myc downstream-regulated gene 2; PCNA, proliferating cell nuclear antigen; SA, substitution of serine residues to alanine on vimentin; *VIM*, vimentin.

(17, 18, 21, 25, 26). These findings indicated that mitotic IF phosphorylation is essential for the efficient separation of the two daughter cells. The presence of the IF bridge presented the cell pair with two options. In the first option, the IF bridge could be torn apart presumably by cell adhesion-dependent traction force (27) to allow the completion of cytokinesis (26). In the second option, cytokinesis failed, resulting in the formation of binucleate (multinucleate) cells (21). The physiological significance of IF phosphorylation during cell division for organogenesis and tissue homeostasis, however, has yet to be determined.

We have generated knock-in mice to produce *VIM* alleles in which the serine residues in vimentin that are phosphorylated in mitosis have been replaced with alanine residues (indicated in Fig. 1A). Homozygotic mice bearing such mutations (*VIM*^{SA/SA}) presented with microphthalmia and lens cataract as phenotypes. The heterozygotes (*VIM*^{WT/SA}) showed no obvious phenotype. Compared with WT (*VIM*^{WT/WT}) and *VIM*^{WT/SA} mice, the epithelial cell number was significantly reduced in lenses from *VIM*^{SA/SA} mice. We observed not only binucleate (multinucleate) cells but also aneuploid cells in *VIM*^{SA/SA} lens, whereas these abnormal cells were not detected in *VIM*^{WT/WT} or *VIM*^{WT/SA} lens. In addition, the mRNA level of the senescence (aging)-related gene was significantly elevated in the lens of *VIM*^{SA/SA}.

EXPERIMENTAL PROCEDURES

Generation of Vimentin Knock-in Mice—A bacterial artificial chromosome clone containing the 129Sv mouse vimentin genome locus was purchased (Mouse bMQ bacterial artificial chromosome library, The Wellcome Trust Sanger Institute). The targeting vector was designed to substitute Ser to Ala in the vimentin head domain at the indicated positions (Fig. 1, A and B). The 5' and 3' homology arms were amplified by PCR. Site-directed mutagenesis was introduced on exon 1 for the substitution. Then they were ligated into the 5' and 3' side of the PGKneobpA-loxP-positive selection marker cassettes, with an MC1DTpA-negative selection marker cassette at the 5' homologous arm to enrich for homologous recombinants. The targeting vector was electroporated into EB3 ES cells with 129 background, as described previously (28, 29).

G418-resistant clones were initially screened by Southern blotting analysis with a unique external probe following EcoRI digestion (see Fig. 1, B and C). Correctly targeted ES clones were microinjected into C57BL/6 blastocysts, which were in turn transferred into foster mothers to obtain chimeric mice. Following germ line transmission, homozygous mutant (*VIM*^{SA/SA}) mice were produced by intercrossing heterozygous (*VIM*^{WT/SA}) mice (Fig. 1, D and E). Mutations were verified by PCR followed by DNA sequencing (Fig. 1F). The mutant mice were backcrossed for more than 10 generations onto a C57BL/6 background. Genotyping was performed by PCR (Fig. 1E) with the following primers: WT (5'-GAT CAG CTC ACC AAC GAC AAG-3'), reverse (5'-TCC TCT GCT ATC CTC CAG ACA-3'), and bpA (5'-TGC ATC GCA TTG TCT GAG TAG-3'). Mice were maintained at the Aichi Cancer Center Research Institute Animal Facility in compliance with the regulations of the Animal Ethics and Animal Care Committees at the Aichi Cancer Center.

Immunoblotting—Samples preparation was described previously (30). After incubation with the desired antibody, PVDF membranes (Immobilon-P, Millipore) were developed using the following detection reagents (Western Lightning Chemiluminescence Reagent plus, PerkinElmer Life Sciences, or Super-Signal West Femto Maximum Sensitivity Substrate, or Thermo Fisher Scientific).

In Situ Hybridization—*In situ* hybridization on whole-mount embryos was performed using digoxigenin-labeled riboprobes as described (31). Templates were cloned from cDNA by PCR amplification with the following primers: vimentin, 5'-atgtctaccagtgctgtg-3' and 5'-cgacatcacgcaggga-3', and desmin, 5'-cgaggctacagcaaca-3' and 5'-tgctctctctctctctct-3'.

Histology and Immunohistochemistry—Fixation and H&E staining of histological sections was performed according to standard protocols. For immunohistochemistry, 3,3'-diaminobenzidine staining was performed with a kit (Dako EnVision+ System-HRP Labeled Polymer, Dako), according to the manufacturer's protocol.

Immunostaining—Paraformaldehyde-fixed tissue slides were deparaffinized, microwaved in 10 mM citrate buffer, pH 6.0, for 15 min, and then blocked in 5% (v/v) donkey serum in TBST for 1 h. Sections were incubated with primary antibodies overnight at 4 °C followed by TBST wash and then incubated with appropriate secondary antibodies (Invitrogen) for 1 h at room temperature.

Cultured cells were grown on coverslips (Iwaki Glass Co., Ltd.) and immunostained with the following modifications: fixation, with 1% (w/v) formaldehyde in PBS for 15 min at room temperature followed by permeabilization with 0.2% (v/v) Triton X-100 for 15 min or with 100% methanol at -20 °C for 10 min; blocking, with 1% (w/v) BSA/PBS for 15 min; primary antibodies, for 1 h at room temperature; secondary antibodies for 30 min. DNA was also stained with 1 μg/ml DAPI.

Fluorescence images were obtained by confocal microscopy (LSM 510 META, Carl Zeiss) and equipped with a microscope (Axiovert 200 M, Carl Zeiss), a Plan Apochromat 40×/1.3 NA, 63×/1.4 NA, and 100×/1.4 NA oil immersion lens, a Plan Apochromat 150×/1.35 NA glycerol immersion lens, and LSM Image Browser software (Carl Zeiss).

Fig. 5A was obtained by using the DeltaVision system (Applied Precision), as described previously (32), equipped with a microscope (IX70, Olympus), a Plan Apochromat 100×/1.40 NA oil immersion lens (Olympus), and a cooled charge-coupled device camera (CoolSNAP HQ, Photometrics). The images were obtained with 0.2-μm intervals in a z section, deconvolved, and integrated with softWoRx software (Applied Precision).

FISH—Mouse eyes were fixed with 4% (w/v) paraformaldehyde in PBS overnight at 4 °C and embedded in paraffin. 5-μm-thick sections were prepared and mounted. Slides were deparaffinized and then treated with 0.1% (w/v) pepsin, 0.1 N HCl for 15 min. FISH probes were mounted with specimen, denatured for 10 min at 90 °C, and then hybridized overnight at 37 °C. After hybridization, slides were washed stringently in 50% formamide, 2× saline sodium citrate (SSC), and 1× SSC. DNA was also stained with 1 μg/ml DAPI.

Cytokinetic Failure Induces Aneuploidy and Aging

Fluorescence image was captured with a fluorescence microscope (Leica CW-4000). The mouse two-color FISH probe (Chromosome 12 probe; labeled with Spectrum Green, chromosome 19 probe; labeled with Cy3) was purchased from Chromosome Science Labo Inc. (Sapporo, Japan).

For the cultured cells, some modifications were made. In brief, cells were fixed with Carnoy's fixative (3:1 methanol/glacial acetic acid) at room temperature for 5 min with three changes before FISH probes were hybridized to the samples.

Antibodies—The following primary antibodies were used: polyclonal guinea pig anti-vimentin (Progen; Germany); monoclonal rabbit anti-desmin (Y266, Abcam, Cambridge, UK); monoclonal mouse anti-GFAP (GA5, Cell Signaling Technology, Beverly, MA); monoclonal mouse anti-nestin (Millipore, Billerica, MA); polyclonal rabbit anti-HSP70 (D69; Cell Signaling Technology, Beverly, MA); HRP-conjugated polyclonal rabbit anti- α -tubulin (Abcam, Cambridge, UK); monoclonal rat anti E-cadherin (ECCD2, Cell Signaling Technology, Beverly, MA); monoclonal mouse anti β -catenin (Transduction Laboratories, Lexington, KY); polyclonal rabbit anti-AQP0/MIP (Alpha Diagnostic International, San Antonio, TX); polyclonal rabbit anti- γ -tubulin (ab11321, Abcam, Cambridge, UK); polyclonal goat anti-vimentin (25); monoclonal rabbit anti-vimentin (D21H3, Cell Signaling Technology, Beverly, MA); monoclonal mouse anti- α -tubulin (B-5-1-2, Sigma); polyclonal rabbit anti-PCNA (ab15497, Abcam, Cambridge, UK); and monoclonal anti- γ -tubulin (GTU-88, Sigma). Primary antibodies were detected using species-specific secondary antibodies conjugated to either Alexa Fluor 488 or 555 (Invitrogen).

Quantitative RT-PCR—Total RNA was prepared from eye lenses using TRIzol[®] (Invitrogen) in accordance with the manufacturer's instructions. Total RNA was reverse-transcribed using SuperScript[®] VILO[™] cDNA synthesis kit (Invitrogen). TaqMan analysis was performed. Primer sequences for p16^{Ink4a} and p19^{Arf} were as published (33). Other primers are the TaqMan[®] Gene Expression Assays by Applied Biosystems: E2f1 (Mm00432936_m1), p15 (Mm00483241_m1), p21 (Mm04205640_g1), GAPDH (Mm99999915_g1), and Ndr2 (Mm00443481_g1).

Primary Cell Culture—Primary lens epithelial cell cultures were established by microdissecting the anterior lens capsule and then culturing on collagen I-coated plastic dish (BD Biosciences) with Dulbecco's modified Eagle's medium supplemented with 10% (v/v) FCS and antibiotics. Sequentially, they were replaced on collagen I-coated coverslips (Iwaki Glass Co., Ltd.) and cultured for a total of 7 days from the harvest, followed by the fixation.

Transmission Electron Microscopy of Lens Fiber Cells—The fixation was based on the following standard method with some modifications for the equatorial section. Lens was fixed with 2% fresh formaldehyde and 2.5% glutaraldehyde in 0.1 M sodium cacodylate buffer, pH 7.4, for 2 h at room temperature. After washing with 0.1 M cacodylate buffer, pH 7.4, they were post-fixed with ice-cold 1% OsO₄ in the same buffer for 2 h. The samples were rinsed with distilled water, stained with 0.5% aqueous uranyl acetate for 2 h or overnight at room temperature, dehydrated with ethanol and propylene oxide, and embedded in Poly/Bed 812 (Polysciences, Inc.). Then ultrathin sec-

tions were cut through the lens equator, double stained with uranyl acetate and Reynolds's lead citrate, and viewed with a transmission electron microscope (JEM-1010; JEOL) with a charge-coupled device camera (BioScan model 792; Gatan, Inc.) at an accelerating voltage of 100 kV.

Statistical Analyses—Mean values \pm S.E. were calculated and used to test for significance between treatments in each dataset using the two-tailed Student's *t* test (Graph Pad software). Differences were considered significant when *, $p < 0.05$; **, $p < 0.01$; and ***, $p < 0.001$.

RESULTS

Lens Disorder in $VIM^{SA/SA}$ Mice—Knock-in mice were generated that only expressed vimentin mutated at Ser-6, Ser-24, Ser-38, Ser-46, Ser-55, Ser-64, Ser-65, Ser-71, Ser-72, Ser-82, and Ser-86 to Ala (Fig. 1, A–F). These serine residues in mouse vimentin have been identified as phosphorylation sites during mitosis. Western blot analyses of embryos showed no significant difference in vimentin protein levels between WT ($VIM^{WT/WT}$), heterozygous ($VIM^{WT/SA}$), and homozygous ($VIM^{SA/SA}$) mice (Fig. 1F). Next, we compared the expression patterns of vimentin and desmin in $VIM^{WT/WT}$ and $VIM^{SA/SA}$ embryos. There were only marginal differences in vimentin and desmin expression, as judged by *in situ* hybridization of mouse whole embryos at E8.5 (Fig. 2A) and E9.5 (Fig. 2B). These data collectively indicate the successful generation of vimentin mutant mice.

$VIM^{SA/SA}$ mice were viable, but the eyes were microphthalmic, and the lenses were smaller than those in littermate controls (Fig. 2C). The gross morphology and histology of the eye tissues were unchanged for $VIM^{WT/WT}$ and $VIM^{WT/SA}$ mice (Fig. 2C). Lens cataract was observed in $VIM^{SA/SA}$ mice at 11 months old, whereas $VIM^{WT/WT}$ and $VIM^{WT/SA}$ mice all had clear lenses (Fig. 2D). As shown in Fig. 2E, we observed no redundant protein expression of desmin, GFAP, and nestin (with which vimentin can form heteropolymeric filaments) (3) in $VIM^{SA/SA}$ lens. The fact that the lens is the tissue where vimentin is the most abundantly expressed (Fig. 2F) likely explains the cataract phenotype in $VIM^{SA/SA}$ mice.

Binucleation and Aneuploidy in $VIM^{SA/SA}$ Lens—A single layer of epithelial cells covers the anterior hemisphere of the lens. The cells in the central zone of the epithelium (anterior region) rarely undergo cell division, but at the lens equator there is a band of dividing cells termed the germinative zone in the epithelium (equatorial region). The progeny of these cells in the germinative zone of the equatorial region differentiate into lens fiber cells, a process that starts in the transitional zone of the equatorial region (34). The immunohistochemical analyses with anti-PCNA (which stains active DNA replication sites in cells; Fig. 3A) identified the germinative zone (34).

Histological changes were observed in both the anterior (Fig. 3, B and C) and equatorial regions (Fig. 4, A and B) of $VIM^{SA/SA}$ lenses. The number of lens epithelial cells was significantly decreased in $VIM^{SA/SA}$ mice, compared with $VIM^{WT/WT}$ or $VIM^{WT/SA}$ mice. In contrast, there was no significant difference between similar regions in $VIM^{WT/WT}$ and $VIM^{WT/SA}$ mice. Because binucleation (multinucleation) was observed in tissue culture cells expressing phosphorylation-compromised vimen-

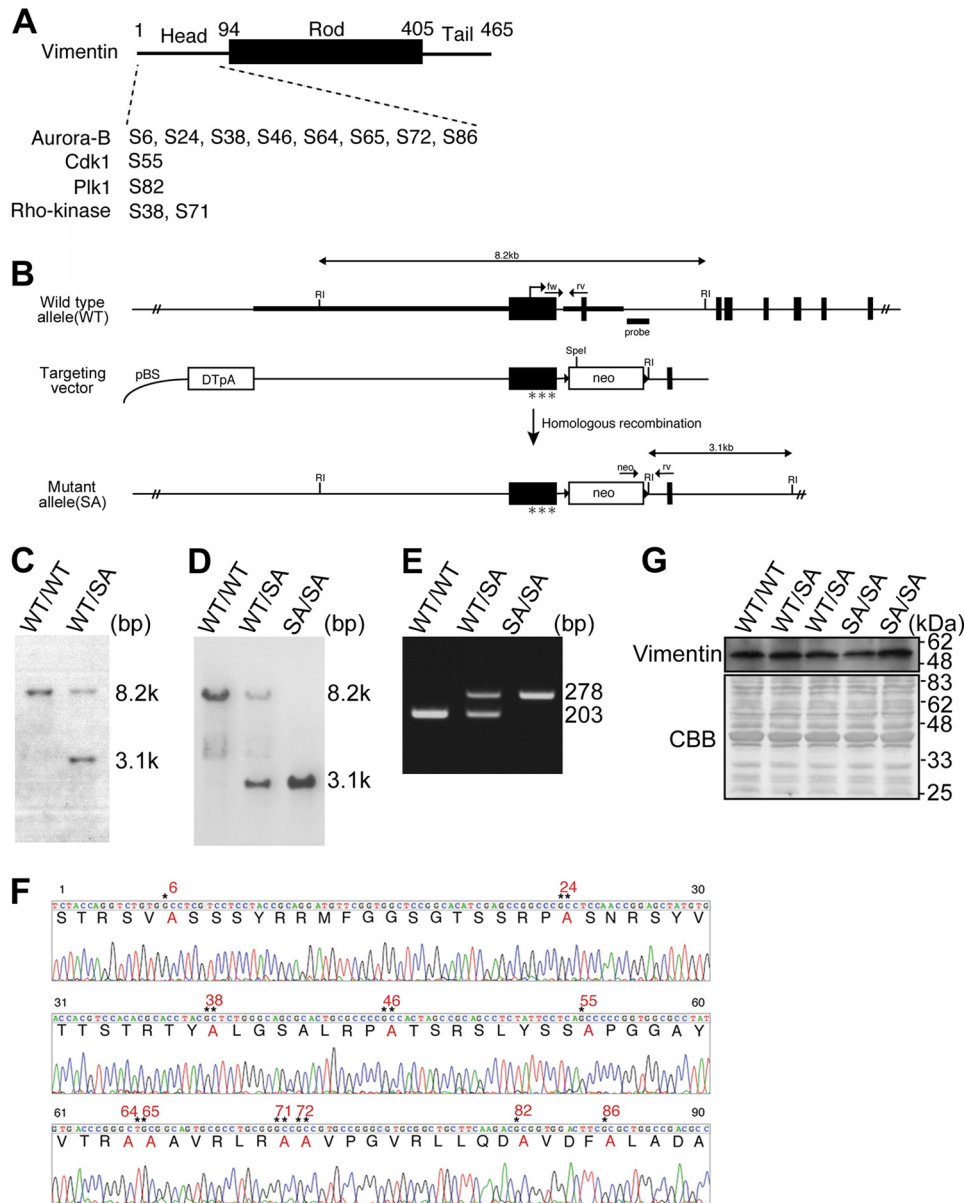


FIGURE 1. Generation of knock-in mice ($VIM^{SA/SA}$) where two VIM alleles are mutated at mitosis-specific phosphorylation sites to Ala. *A*, schematic featuring mitosis-specific vimentin phosphorylation sites on mouse vimentin. Their responding kinases are also shown. *B*, diagram of the VIM genomic locus is shown as follows: WT allele with EcoRI (R_I) restriction maps, exons (black box), and translation initiation point (hooked arrow); targeting vector, including mutated exon1 (with asterisks), and inserting *neo* gene; mutant allele by homologous recombination. Genotyping probes for Southern blot (*bar*) and the PCR primers (*arrows*) are also illustrated. *C* and *D*, Southern blotting of EcoRI-digested genomic DNA from ES clones (*C*) and tails from offspring (*D*). About 8.2- or 3.1-kbp fragment is derived from EcoRI-digested genomic DNA of a VIM^{WT} or *neo*-inserted VIM^{SA} allele, respectively. *E*, PCR genotyping of offspring. The 278- or 203-bp fragment is derived from mRNA of a VIM^{SA} or VIM^{WT} allele, respectively. *F*, sequence of mutation sites on $VIM^{SA/SA}$ were checked as described under "Experimental Procedures." *G*, Western blot analyses with extracts from embryos. After blotting, the membrane was stained with Coomassie Brilliant Blue (CBB). *, $p < 0.05$; **, $p < 0.01$; ***, $p < 0.001$.

tin (21), lenses from $VIM^{SA/SA}$ were stained with E-cadherin, β -catenin (the markers of cell-cell boundaries), and DAPI (nucleus). In both anterior (Fig. 3, *D* and *E*) and equatorial (Fig. 4, *C* and *D*) regions of $VIM^{WT/WT}$ or $VIM^{WT/SA}$ lens epithelium, each cell had one nucleus. In contrast, binucleate (multinucleate) cells were observed in $VIM^{SA/SA}$ lens epithelium. Approximately 13 and 1% of cells each had two nuclei in the anterior (Fig. 3, *D* and *E*) and equatorial (Fig. 4, *C* and *D*) regions, respectively. FISH analyses using mouse chromosome 12 (*green*) and 19 (*red*) probes were used to determine chromosomal instability (CIN) in $VIM^{SA/SA}$ lenses. Approximately 3 and 17% of nuclei in the anterior (Fig. 3, *F* and *G*) and equatorial (Fig. 4, *E* and *F*)

regions, respectively, of $VIM^{SA/SA}$ lens epithelial cells had more than two FISH signals per chromosome. Aneuploid cells were not detected in $VIM^{WT/WT}$ or $VIM^{WT/SA}$ lens epithelial cells.

To analyze the mechanism by which CIN occurs in lens epithelial cells, we analyzed primary cultures of lens epithelial cells. $VIM^{SA/SA}$ -derived primary culture cells exhibited not only binucleation (Fig. 5*A*) but also aneuploidy (Fig. 5*B*). These phenomena were rarely observed in $VIM^{WT/WT}$ - or $VIM^{WT/SA}$ -derived primary culture cells. The binucleate cells in primary cell cultures derived from $VIM^{SA/SA}$ lenses possessed four centrosomes (Fig. 5*A*) consistent with cytokinetic failure causing binucleation (multinucleation) just like T24 cultured cells

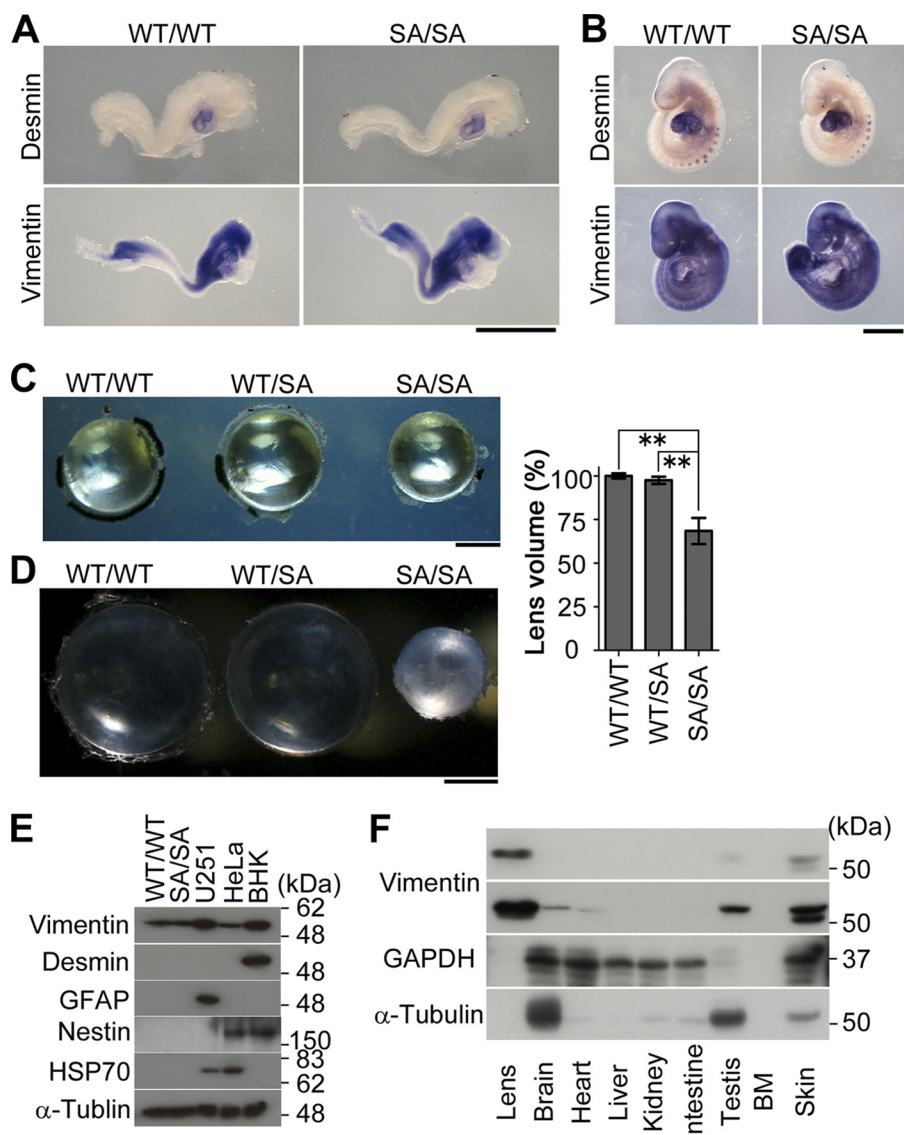


FIGURE 2. **Optical disorder in knock-in mice ($VIM^{SA/SA}$).** *A* and *B*, *in situ* hybridization analyses of mouse whole embryos at E8.5 (*A*) and E9.5 (*B*) using vimentin and desmin probes. *C* and *D*, lens from 4-month-old (*C*) or 11-month-old (*D*) mice. *Bar graph* shows the quantification of the volume of lens, normalized to $VIM^{WT/WT}$ lens ($n = 5$ mice per genotype; *C*). The volume of 4-month-old lens (*C*) was calculated with the following mathematical formula: $V = 4\pi Rr^2/3$ (R , major radius; r , minor axis). *E*, total lens lysates (20 μ g) prepared from 4-month-old mice were analyzed by Western blotting. The lysates of U251, HeLa, and baby hamster kidney (BHK) cells were loaded as positive controls. *F*, vimentin expression pattern of indicated mouse tissues. 15 μ g of total protein are applied in each lane. Scale bars, 500 μ m (*A* and *B*) or 1 mm (*C* and *D*). **, $p < 0.01$.

that express similar phosphorylation-compromised vimentin mutants (21). Does this account for aneuploidy in $VIM^{SA/SA}$ lens epithelial cells? Extra centrosomes have been reported to be sufficient to induce chromosome missegregation (such as lagging chromosomes) during cell division (35). Interestingly, tetraploid cells with four centrosomes showed a high frequency of chromosome missegregation whereas tetraploid cells with two centrosomes decreased to a level observed in diploid cells with two centrosomes (35). These observations led us to propose the following model. Lens epithelial cells in $VIM^{SA/SA}$ mice form an IF bridge, which induces binucleation (multi-nucleation) due to cytokinetic failure. The binucleation (multi-nucleation) results in abnormal numbers of centrosomes per cell, which in turn promotes aneuploidy. Given the regional differences in the frequency of cell division rates in the anterior and equatorial regions of the lens, this could explain why there

is more binucleation (early event) in the central region and more aneuploidy (later event) in the equatorial zone (Fig. 3 versus Fig. 4).

Premature Aging in $VIM^{SA/SA}$ Lens—How CIN induces microphthalmia and cataract in $VIM^{SA/SA}$ mice is an important question. As judged by TUNEL staining, it is less likely that CIN promotes apoptosis in $VIM^{SA/SA}$ lens.⁴ Table 1 summarizes the time course of the appearance of the lens abnormalities. Two months after birth, all lens abnormalities have started to appear in some $VIM^{SA/SA}$ mice. The abnormalities in lens size and chromosomal stability were observed in all $VIM^{SA/SA}$ mice by 3 months, whereas it took almost 1 year before all $VIM^{SA/SA}$ mice exhibited cataract phenotype. These observa-

⁴ H. Tanaka and M. Inagaki, unpublished observations.

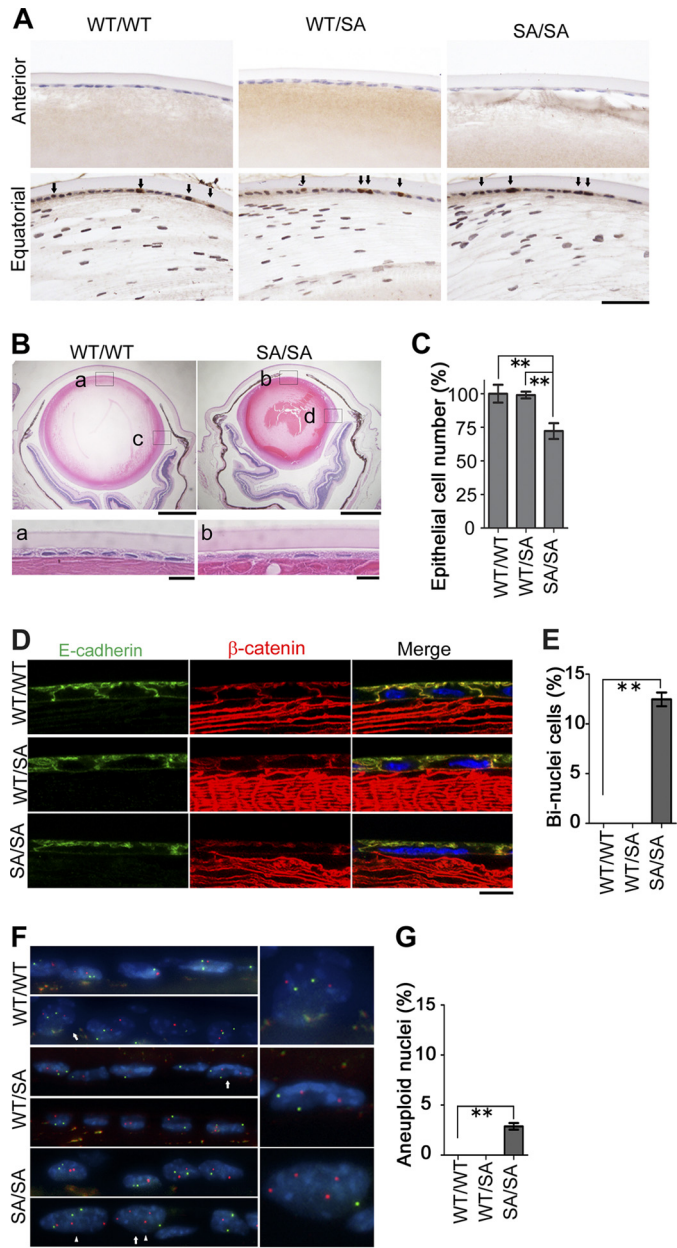


FIGURE 3. Changes in the epithelial cells in the anterior region of *VIM^{SA/SA}* lenses. *A*, active dividing site of lens epithelium. Cells in lens tissue were stained with anti-PCNA. *Arrows* indicate PCNA-positive nuclei. *B*, microphthalmia in the *VIM^{SA/SA}* mice. Lens from 4-month-old *VIM^{WT/WT}* or *VIM^{SA/SA}* mice was stained with H&E. Magnified images of anterior or equatorial regions of lens are also shown below (*a* and *b*) or in Fig. 4*A* (*c* and *d*), respectively. *C*, *bar graph* shows the cell number of epithelium per $500 \times 100 \mu\text{m}$ area, normalized to *VIM^{WT/WT}* mice ($n = 3$ mice per genotype); we observed at least 10 sections per each lens for the calculation. *D* and *E*, immunostaining (*D*) of lens epithelial cells with anti-E-cadherin (green), anti- β -catenin (red), and DAPI (blue; nuclei). *Bar graph* (*E*) shows the percentage of binucleate cells per $500 \times 100 \mu\text{m}$ area; we observed at least 10 sections per each lens for the calculation ($n = 3$ mice per genotype). *E–G*, FISH analyses of nuclei in each genotype of mice. Green or red color represents mouse chromosome 12 or 19, respectively (*G*). Magnified images of nuclei indicated as *arrows* are shown at right. *Arrowheads* indicate aneuploid nuclei (*F*). Quantification of aneuploid nuclei is also shown (*G*; $n = 3$ mice per genotype). Scale bars, $50 \mu\text{m}$ (*A*), $50 \mu\text{m}$ (*B*, upper), $40 \mu\text{m}$ (*B*, lower), or $10 \mu\text{m}$ (*D* and *F*). **, $p < 0.01$.

tions suggested that lens cataract followed after CIN in *VIM^{SA/SA}* lenses.

To examine lens fiber morphology in detail, lens epithelial cells were costained with anti-AQP0 (also called membrane

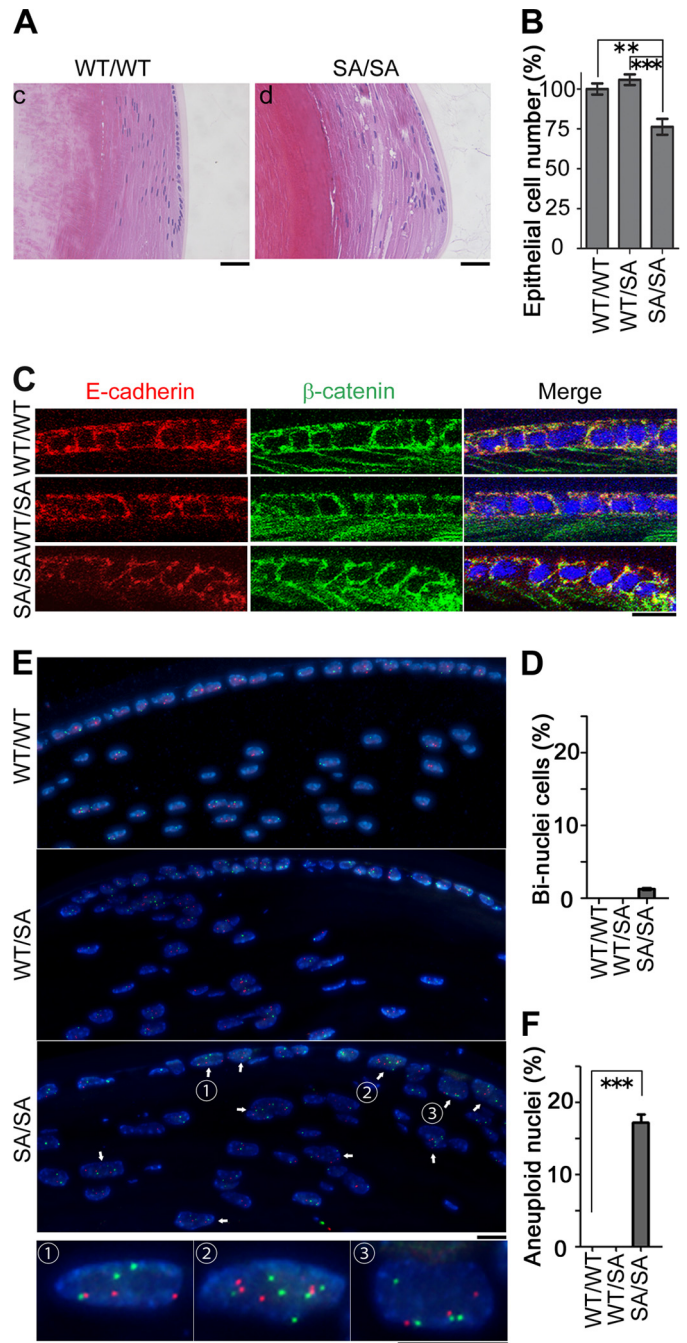


FIGURE 4. Changes in the epithelial cells in the equatorial region of *VIM^{SA/SA}* lenses. *A–F*, histological analyses at equatorial portion of lens were performed according to the legend of Fig. 3. *Bar graphs* show the relative proportion of cell number or binuclear ratio per $300 \times 100 \mu\text{m}$ area; we observed at least 10 sections per each lens for the calculation (*B* and *D*). Scale bars, $40 \mu\text{m}$ (*A*) or $10 \mu\text{m}$ (*C* and *E*). **, $p < 0.01$; ***, $p < 0.001$.

intrinsic protein (MIP)) and anti-vimentin. Lens fiber cells were disorganized at 4 months as seen by the AQP0 staining (Fig. 6, *A* and *B*) after birth when CIN was observed in all *VIM^{SA/SA}* mice (also see Table 1). The vimentin network was also disorganized, but no vimentin aggregates were seen (Fig. 6, *A* and *B*).

Inter-fiber spaces were also increased in *VIM^{SA/SA}* lens (Fig. 6, *A* and *B*), and in the bow region of the lens, the characteristic distribution of the fiber cell nuclei was disrupted (Figs. 4*A* and 6*B*). Vacuoles (area devoid of cellular materials; Fig. 4*A*) were

Cytokinetic Failure Induces Aneuploidy and Aging

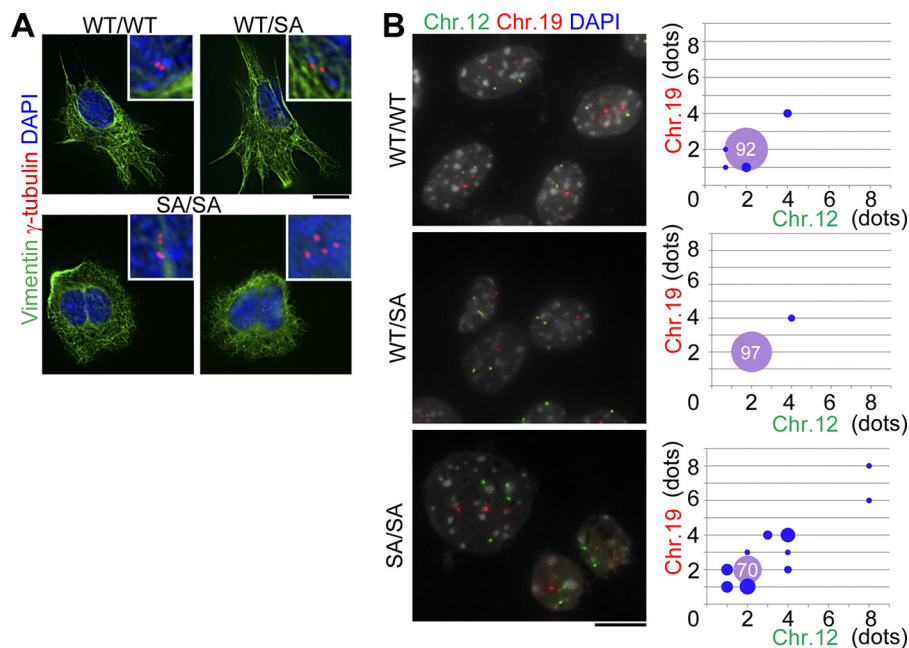


FIGURE 5. Analysis of primary lens epithelial cell culture. *A* and *B*, lens epithelial cells were primarily cultured for 7 days and then subjected to immunostaining (*A*) or FISH analyses (*B*). *Upper insets* indicate magnification images around centrosomes in each cell (*A*). Cells were classified as the numbers of chromosome (*Chr.*) 12 and 19 according to FISH data (*left photographs* in *B*). The proportion of each category is indicated as the size of circle (*right scattered graph* in *B*; $n = 100$ nuclei per genotype). The percentage of normal diploid (with each two chromosomes) is shown in the violet circle (*right graph* in *B*). Scale bars, 10 μm (*A* and *B*).

TABLE 1
Age-dependent lens abnormality in $Vim^{SA/SA}$ mice

	Abnormal lens size	Lens fiber disorientation	Bi nuclei	Aneuploidy	Cataract
Homozygous (SA/SA)					
2 months	$n = 1/3$	$n = 1/3$	$n = 1/3$	$n = 1/3$	$n = 1/3$
3 months	$n = 4/4$	$n = 4/4$	$n = 4/4$	$n = 4/4$	$n = 1/4$
4 months	$n = 4/4$	$n = 4/4$	$n = 4/4$	$n = 4/4$	$n = 2/4$
6 months	$n = 4/4$	$n = 4/4$	$n = 4/4$	$n = 4/4$	$n = 2/4$
8 months	$n = 4/4$	$n = 4/4$	$n = 4/4$	$n = 4/4$	$n = 3/4$
12 months	$n = 3/3$	$n = 3/3$	$n = 3/3$	$n = 3/3$	$n = 3/3$
Heterozygous (WT/SA)					
2 months	$n = 0/3$	$n = 0/3$	$n = 0/3$	$n = 0/3$	$n = 0/3$
3 months	$n = 0/4$	$n = 0/4$	$n = 0/4$	$n = 0/4$	$n = 0/4$
4 months	$n = 0/4$	$n = 0/4$	$n = 0/4$	$n = 0/4$	$n = 0/4$
6 months	$n = 0/4$	$n = 0/4$	$n = 0/4$	$n = 0/4$	$n = 0/4$
8 months	$n = 0/4$	$n = 0/4$	$n = 0/4$	$n = 0/4$	$n = 0/4$
12 months	$n = 0/3$	$n = 0/3$	$n = 0/3$	$n = 0/3$	$n = 0/3$
Wild type (WT/WT)					
2 months	$n = 0/3$	$n = 0/3$	$n = 0/3$	$n = 0/3$	$n = 0/3$
3 months	$n = 0/4$	$n = 0/4$	$n = 0/4$	$n = 0/4$	$n = 0/4$
4 months	$n = 0/4$	$n = 0/4$	$n = 0/4$	$n = 0/4$	$n = 0/4$
6 months	$n = 0/4$	$n = 0/4$	$n = 0/4$	$n = 0/4$	$n = 0/4$
8 months	$n = 0/4$	$n = 0/4$	$n = 0/4$	$n = 0/4$	$n = 0/4$
12 months	$n = 0/3$	$n = 0/3$	$n = 0/3$	$n = 0/3$	$n = 0/3$

also apparent in $VIM^{SA/SA}$ lenses. Such observations are consistent with other mouse models that develop lens cataract (36–39).

The cross-sectional profiles of fiber cells at the lens equator were analyzed by transmission electron microscopy (40). The profiles of both $VIM^{WT/WT}$ or $VIM^{WT/SA}$ lens fiber cells were very regular maintaining their characteristic hexagonal geometry over 11 months (Fig. 6C). $VIM^{SA/SA}$ lens fiber cells were, however, irregular both in size and shape. Size variation was very apparent as too was the disorganized membrane morphology manifested in, for example, irregular membrane processes (Fig. 6C). In samples from 11-month-old $VIM^{SA/SA}$ mice, the

fiber cell boundaries were apparently lost in some areas (see a *right lowest photograph* in Fig. 6C), which we interpret as a degenerative process (41). Even with the increased resolution of the electron microscope, no electron dense aggregates were observed in the $VIM^{SA/SA}$ lenses. The observed changes in the plasma membranes of the $VIM^{SA/SA}$ lenses resemble those seen in age-related cataracts (41).

Given this comparison, real time PCR analyses to monitor mRNA levels of several senescence (aging)-related genes (p21, Ndr2, p16^{Ink4a}, and p19^{Arf}) were performed on lens samples. The induction of p21 was recently reported to promote senescence in lens epithelial cells leading to cataract formation (42). N-myc downstream regulated gene 2 (Ndr2) is considered to be a lens-specific senescent marker (43). Two aging biomarkers of various human and rodent tissues, p16^{Ink4a} and p19^{Arf} (44), were also reported to be induced in eye tissue of hypomorphic BubR1 ($BubR1^{H/H}$) progeroid mice (45). The elevation of p21 promotes senescence of lens epithelial cells and cataract formation, whereas the later elevation of p16^{Ink4a} and p19^{Arf} is related to age-related tissue deterioration (42).

As shown in Fig. 6D, mRNA expression of p21 or Ndr2 was significantly elevated in lens of 4-month-old $VIM^{SA/SA}$ mice, compared with the littermate control. 12 months after birth, transcript levels of not only p21 and Ndr2 but also p16^{Ink4a} and p19^{Arf} were significantly higher in $VIM^{SA/SA}$ lens than in $VIM^{WT/WT}$ or $VIM^{WT/SA}$ lens (Fig. 6E). These data suggest that premature cataract formation might represent a progeroid-like lens phenotype in $VIM^{SA/SA}$ mice.

DISCUSSION

In this study, we have analyzed the physiological effects of the expression of a vimentin mutant that will remain unphosphorylated during cell division by replacing with alanine all the ser-

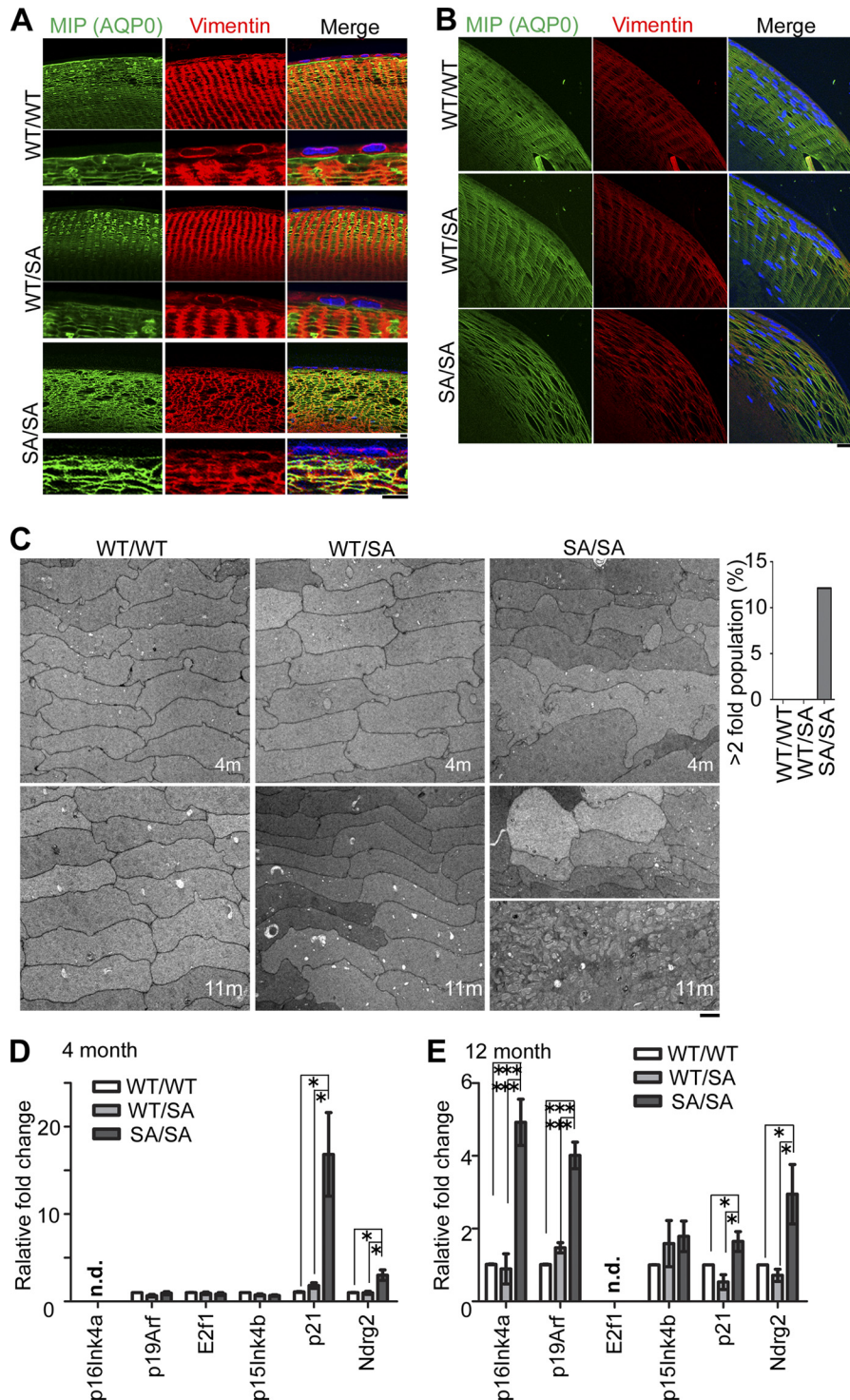


FIGURE 6. Progeria-like phenotypes apparent in $VIM^{SA/SA}$ lenses. *A* and *B*, disorganization of lens fiber cells in $VIM^{SA/SA}$ mice. Anterior (*A*) or equatorial (*B*) lens fiber cells from 4-month-old mice were immunostained with anti-MIP (AQP0; green), anti-vimentin (red), and DAPI (blue; nuclei). *C*, electron micrographs of lens at 4 (upper) or 11 (lower) months of age. The dispersion in the size distribution was evaluated as the percentage of cells >2 larger than the average size of cells (right graph). *D* and *E*, mRNA expression of the indicated genes were analyzed through quantitative RT-PCR using the lens of 4-month-old (*D*) or 12-month-old (*E*) mice ($n = 5$ mice per genotype). *n.d.* means "no detected signals." Scale bars, 30 μm (*A*, upper) or 10 μm (*A*, lower) and *B* and *C*. *, $p < 0.05$; ***, $p < 0.001$.

ine residues known to be phosphorylated in mitosis. Binucleate (multinucleate) epithelial cells were observed in the lenses of $VIM^{SA/SA}$ mice (Figs. 3 and 4), mimicking the observations made with T24 cultured cells that expressed phosphorylation-compromised vimentin. Pairs of cells remained connected by an IF bridge, which subsequently induced cytokinetic failure

(21). We also found aneuploid lens epithelial cells in $VIM^{SA/SA}$ mice (Figs. 3 and 4), which was unexpected. Perhaps this is due to the presence of additional centrosomes in the binucleated cells (as discussed above). CIN accelerates premature aging, and in $VIM^{SA/SA}$ mice this was manifested as cataracts, the classic age-related phenotype of the eye lens.

Cytokinetic Failure Induces Aneuploidy and Aging

Congenital cataracts can be caused by vimentin mutations, for example, the E151K ($VIM^{WT/E151K}$) mutation in the vimentin rod domain (46). Magin and co-workers (47) also reported lens cataract formation in the transgenic mice with vimentin carrying R113C mutation (VimR113C). The cataract pathology observed for both these mutations in the vimentin rod domain is different from that reported here in several respects. Both are autosomal dominant mutations (46, 47). In contrast, no cataract pathology was observed in $VIM^{WT/SA}$ mice. The inheritance is therefore recessive and not dominant in character. Rod domain vimentin mutants also formed protein aggregates, and the endogenous vimentin network was disrupted (46, 47). Such consequences were rarely, if at all, observed in both $VIM^{WT/SA}$ and $VIM^{SA/SA}$ mice (Fig. 6). This observation is consistent with our previous finding that SA mutants can normally form vimentin filament networks in interphase cells (25). Finally, the expression of HSP70 was elevated in response to abnormal vimentin structures such as protein aggregates in transgenic VimR113C mice (47), but such a phenomenon was not observed in the lenses of $VIM^{SA/SA}$ mice (Fig. 2E). Taken together, it is less likely that the expression of phosphorylation-compromised vimentin may induce abnormal vimentin filament structure and subsequently lens cataract.

In conclusion, this study documents for the first time the physiological importance of vimentin phosphorylation during cell division in the lens. It also paves the way for future studies evaluating the relationship between CIN and premature aging.

Acknowledgments—We thank Drs. H. Niwa for EB3 ES cell line, R. R. Behringer for the PGKneobpA-loxP plasmid, and T. Yagi for the pMCDTPa plasmid. We are grateful to Dr. R. A. Quinlan (Durham University, United Kingdom) not only for teaching the methods of lens primary culture but also for critical comments on the manuscript.

REFERENCES

1. Eriksson, J. E., Opal, P., and Goldman, R. D. (1992) Intermediate filament dynamics. *Curr. Opin. Cell Biol.* **4**, 99–104
2. Fuchs, E., and Weber, K. (1994) Intermediate filaments: structure, dynamics, function, and disease. *Annu. Rev. Biochem.* **63**, 345–382
3. Eriksson, J. E., Dechat, T., Grin, B., Helfand, B., Mendez, M., Pallari, H. M., and Goldman, R. D. (2009) Introducing intermediate filaments: from discovery to disease. *J. Clin. Invest.* **119**, 1763–1771
4. Quinlan, R. A., Brenner, M., Goldman, J. E., and Messing, A. (2007) GFAP and its role in Alexander disease. *Exp. Cell Res.* **313**, 2077–2087
5. Pekny, M., and Lane, E. B. (2007) Intermediate filaments and stress. *Exp. Cell Res.* **313**, 2244–2254
6. Capetanaki, Y., Bloch, R. J., Kouloumenta, A., Mavroidis, M., and Psarras, S. (2007) Muscle intermediate filaments and their links to membranes and membranous organelles. *Exp. Cell Res.* **313**, 2063–2076
7. Song, S., Landsbury, A., Dahm, R., Liu, Y., Zhang, Q., and Quinlan, R. A. (2009) Functions of the intermediate filament cytoskeleton in the eye lens. *J. Clin. Invest.* **119**, 1837–1848
8. Ivaska, J., Pallari, H. M., Nevo, J., and Eriksson, J. E. (2007) Novel functions of vimentin in cell adhesion, migration, and signaling. *Exp. Cell Res.* **313**, 2050–2062
9. Inagaki, M., Matsuoka, Y., Tsujimura, K., Ando, S., Tokui, T., Takahashi, T., and Inagaki, N. (1996) Dynamic property of intermediate filaments: regulation by phosphorylation. *BioEssays* **18**, 481–487
10. Sihag, R. K., Inagaki, M., Yamaguchi, T., Shea, T. B., and Pant, H. C. (2007) Role of phosphorylation on the structural dynamics and function of types III and IV intermediate filaments. *Exp. Cell Res.* **313**, 2098–2109
11. Inagaki, M., Nishi, Y., Nishizawa, K., Matsuyama, M., and Sato, C. (1987) Site-specific phosphorylation induces disassembly of vimentin filaments *in vitro*. *Nature* **328**, 649–652
12. Goto, H., and Inagaki, M. (2007) Production of a site- and phosphorylation state-specific antibody. *Nat. Protoc.* **2**, 2574–2581
13. Nishizawa, K., Yano, T., Shibata, M., Ando, S., Saga, S., Takahashi, T., and Inagaki, M. (1991) Specific localization of phosphointermediate filament protein in the constricted area of dividing cells. *J. Biol. Chem.* **266**, 3074–3079
14. Goto, H., Kosako, H., and Inagaki, M. (2000) Regulation of intermediate filament organization during cytokinesis: possible roles of Rho-associated kinase. *Microsc. Res. Tech.* **49**, 173–182
15. Izawa, I., and Inagaki, M. (2006) Regulatory mechanisms and functions of intermediate filaments: a study using site- and phosphorylation state-specific antibodies. *Cancer Sci.* **97**, 167–174
16. Matsuoka, Y., Nishizawa, K., Yano, T., Shibata, M., Ando, S., Takahashi, T., and Inagaki, M. (1992) Two different protein kinases act on a different time schedule as glial filament kinases during mitosis. *EMBO J.* **11**, 2895–2902
17. Goto, H., Yasui, Y., Kawajiri, A., Nigg, E. A., Terada, Y., Tatsuka, M., Nagata, K., and Inagaki, M. (2003) Aurora-B regulates the cleavage furrow-specific vimentin phosphorylation in the cytokinetic process. *J. Biol. Chem.* **278**, 8526–8530
18. Kawajiri, A., Yasui, Y., Goto, H., Tatsuka, M., Takahashi, M., Nagata, K., and Inagaki, M. (2003) Functional significance of the specific sites phosphorylated in desmin at cleavage furrow: Aurora-B may phosphorylate and regulate type III intermediate filaments during cytokinesis coordinately with Rho-kinase. *Mol. Biol. Cell* **14**, 1489–1500
19. Tsujimura, K., Ogawara, M., Takeuchi, Y., Imajoh-Ohmi, S., Ha, M. H., and Inagaki, M. (1994) Visualization and function of vimentin phosphorylation by cdc2 kinase during mitosis. *J. Biol. Chem.* **269**, 31097–31106
20. Chou, Y. H., Bischoff, J. R., Beach, D., and Goldman, R. D. (1990) Intermediate filament reorganization during mitosis is mediated by p34cdc2 phosphorylation of vimentin. *Cell* **62**, 1063–1071
21. Yamaguchi, T., Goto, H., Yokoyama, T., Silljé, H., Hanisch, A., Uldschmid, A., Takai, Y., Oguri, T., Nigg, E. A., and Inagaki, M. (2005) Phosphorylation by Cdk1 induces Plk1-mediated vimentin phosphorylation during mitosis. *J. Cell Biol.* **171**, 431–436
22. Goto, H., Kosako, H., Tanabe, K., Yanagida, M., Sakurai, M., Amano, M., Kaibuchi, K., and Inagaki, M. (1998) Phosphorylation of vimentin by Rho-associated kinase at a unique amino-terminal site that is specifically phosphorylated during cytokinesis. *J. Biol. Chem.* **273**, 11728–11736
23. Kosako, H., Amano, M., Yanagida, M., Tanabe, K., Nishi, Y., Kaibuchi, K., and Inagaki, M. (1997) Phosphorylation of glial fibrillary acidic protein at the same sites by cleavage furrow kinase and Rho-associated kinase. *J. Biol. Chem.* **272**, 10333–10336
24. Inada, H., Togashi, H., Nakamura, Y., Kaibuchi, K., Nagata, K., and Inagaki, M. (1999) Balance between activities of Rho kinase and type 1 protein phosphatase modulates turnover of phosphorylation and dynamics of desmin/vimentin filaments. *J. Biol. Chem.* **274**, 34932–34939
25. Yasui, Y., Goto, H., Matsui, S., Manser, E., Lim, L., Nagata, K., and Inagaki, M. (2001) Protein kinases required for segregation of vimentin filaments in mitotic process. *Oncogene* **20**, 2868–2876
26. Yasui, Y., Amano, M., Nagata, K., Inagaki, N., Nakamura, H., Saya, H., Kaibuchi, K., and Inagaki, M. (1998) Roles of Rho-associated kinase in cytokinesis; mutations in Rho-associated kinase phosphorylation sites impair cytokinetic segregation of glial filaments. *J. Cell Biol.* **143**, 1249–1258
27. O'Connell, C. B., Wheatley, S. P., Ahmed, S., and Wang, Y. L. (1999) The small GTP-binding protein Rho regulates cortical activities in cultured cells during division. *J. Cell Biol.* **144**, 305–313
28. Niwa, H., Masui, S., Chambers, I., Smith, A. G., and Miyazaki, J. (2002) Phenotypic complementation establishes requirements for specific POU domain and generic transactivation function of Oct-3/4 in embryonic stem cells. *Mol. Cell Biol.* **22**, 1526–1536
29. Ogawa, K., Matsui, H., Ohtsuka, S., and Niwa, H. (2004) A novel mechanism for regulating clonal propagation of mouse ES cells. *Genes Cells* **9**, 471–477
30. Tanaka, H., Tamura, A., Sekai, M., Hamazaki, Y., and Minato, N. (2011)

- Increased c-Myc activity and DNA damage in hematopoietic progenitors precede myeloproliferative disease in Spa-1-deficiency. *Cancer Sci.* **102**, 784–791
31. Wilkinson, D. G. (ed) (1992) *In Situ Hybridization: A Practical Approach*, pp. 75–83, IRL Press at Oxford University Press, Oxford
 32. Inoko, A., Matsuyama, M., Goto, H., Ohmuro-Matsuyama, Y., Hayashi, Y., Enomoto, M., Ibi, M., Urano, T., Yonemura, S., Kiyono, T., Izawa, L., and Inagaki, M. (2012) Trichoplein and Aurora A block aberrant primary cilia assembly in proliferating cells. *J. Cell Biol.* **197**, 391–405
 33. Krishnamurthy, J., Ramsey, M. R., Ligon, K. L., Torrice, C., Koh, A., Bonner-Weir, S., and Sharpless, N. E. (2006) p16INK4a induces an age-dependent decline in islet regenerative potential. *Nature* **443**, 453–457
 34. Sharma, K. K., and Santhoshkumar, P. (2009) Lens aging: effects of crystallins. *Biochim. Biophys. Acta* **1790**, 1095–1108
 35. Ganem, N. J., Godinho, S. A., and Pellman, D. (2009) A mechanism linking extra centrosomes to chromosomal instability. *Nature* **460**, 278–282
 36. Boyle, D. L., Takemoto, L., Brady, J. P., and Wawrousek, E. F. (2003) Morphological characterization of the α A- and α B-crystallin double knockout mouse lens. *BMC Ophthalmol.* **3**, 3
 37. Liu, H., Du, X., Wang, M., Huang, Q., Ding, L., McDonald, H. W., Yates, J. R., 3rd, Beutler, B., Horwitz, J., and Gong, X. (2005) Crystallin γ B-I4F mutant protein binds to α -crystallin and affects lens transparency. *J. Biol. Chem.* **280**, 25071–25078
 38. Bassuk, J. A., Birkebak, T., Rothmier, J. D., Clark, J. M., Bradshaw, A., Muchowski, P. J., Howe, C. C., Clark, J. L., and Sage, E. H. (1999) Disruption of the Sparc locus in mice alters the differentiation of lenticular epithelial cells and leads to cataract formation. *Exp. Eye Res.* **68**, 321–331
 39. Chang, B., Wang, X., Hawes, N. L., Ojakian, R., Davisson, M. T., Lo, W. K., and Gong, X. (2002) A Gja8 (Cx50) point mutation causes an alteration of α 3 connexin (Cx46) in semi-dominant cataracts of Lop10 mice. *Hum. Mol. Genet.* **11**, 507–513
 40. Nowak, R. B., Fischer, R. S., Zoltoski, R. K., Kuszak, J. R., and Fowler, V. M. (2009) Tropomodulin1 is required for membrane skeleton organization and hexagonal geometry of fiber cells in the mouse lens. *J. Cell Biol.* **186**, 915–928
 41. Michael, R., and Bron, A. J. (2011) The ageing lens and cataract: a model of normal and pathological ageing. *Philos. Trans. R. Soc. Lond. B Biol. Sci.* **366**, 1278–1292
 42. Baker, D. J., Weaver, R. L., and van Deursen, J. M. (2013) p21 both attenuates and drives senescence and aging in BubR1 progeroid mice. *Cell Rep.* **3**, 1164–1174
 43. Zhang, Z. F., Zhang, J., Hui, Y. N., Zheng, M. H., Liu, X. P., Kador, P. F., Wang, Y. S., Yao, L. B., and Zhou, J. (2011) Up-regulation of NDRG2 in senescent lens epithelial cells contributes to age-related cataract in human. *PLoS One* **6**, e26102
 44. Krishnamurthy, J., Torrice, C., Ramsey, M. R., Kovalev, G. I., Al-Regaiey, K., Su, L., and Sharpless, N. E. (2004) Ink4a/Arf expression is a biomarker of aging. *J. Clin. Invest.* **114**, 1299–1307
 45. Baker, D. J., Perez-Terzic, C., Jin, F., Pitel, K. S., Pitel, K., Niederländer, N. J., Jeganathan, K., Yamada, S., Reyes, S., Rowe, L., Hiddinga, H. J., Eberhardt, N. L., Terzic, A., and van Deursen, J. M. (2008) Opposing roles for p16Ink4a and p19Arf in senescence and ageing caused by BubR1 insufficiency. *Nat. Cell Biol.* **10**, 825–836
 46. Müller, M., Bhattacharya, S. S., Moore, T., Prescott, Q., Wedig, T., Herrmann, H., and Magin, T. M. (2009) Dominant cataract formation in association with a vimentin assembly disrupting mutation. *Hum. Mol. Genet.* **18**, 1052–1057
 47. Bornheim, R., Müller, M., Reuter, U., Herrmann, H., Büsow, H., and Magin, T. M. (2008) A dominant vimentin mutant upregulates Hsp70 and the activity of the ubiquitin-proteasome system, and causes posterior cataracts in transgenic mice. *J. Cell Sci.* **121**, 3737–3746